

Article

Near-Graphite Coke Deposit on Nano-HZSM-5 Aggregates for Methanol to Propylene and Butylene Reaction

Yu Sang ¹, Aihua Xing ^{1,*}, Chuanfu Wang ¹, Zhihua Han ¹ and Yulong Wu ²

¹ National Institute of Clean-and-Low-Carbon Energy, Beijing 102209, China; sangyu@nicenergy.com (Y.S.); wangchuanfu@nicenergy.com (C.W.); hanzhizhua@nicenergy.com (Z.H.)

² Institute of Nuclear and New Energy Technology, Tsinghua University, Beijing 100084, China; wylong@tsinghua.edu.cn

* Correspondence: xingaihua@nicenergy.com

Academic Editors: Keith Hohn, Tian-Yi Ma, Jian-Rong (Jeff) Li and Cláudia Gomes Silva

Received: 23 March 2017; Accepted: 18 May 2017; Published: 1 June 2017

Abstract: Nanocrystal HZSM-5 zeolite aggregates with different SiO₂/Al₂O₃ molar ratios were prepared under low temperature and were used to catalyze the conversion of methanol to propylene and butene. The coke location, coke content, and coke species deposited on HZSM-5 aggregates were investigated. The near-graphite carbon on the external surface of HZSM-5 zeolite (SiO₂/Al₂O₃ molar ratio = 400) was distinguished by transmission electron microscopy (TEM) and energy dispersive spectrometer (EDS). The carbon distributions in the micropores and on the external surface of the spent HZSM-5 were revealed by thermogravimetric analysis (TGA) and Brunauer-Emmett-Teller (BET) results. Coke preferred to deposit in the micropores of low SiO₂/Al₂O₃ molar ratio samples (200, 300) with relatively uniform Al distribution, while coke also preferred to deposit on the external surface and in the intergranular spaces of high SiO₂/Al₂O₃ molar ratio sample (400) with an obviously poor Al core and rich Al shell.

Keywords: HZSM-5 zeolite; nanocrystal; aggregate; coke; methanol; propylene and butylene

1. Introduction

Methanol-to-olefins (MTO) is an important process that produces light olefins with non-petroleum resources as feedstock in China [1]. Industrialized MTO process or methanol-to-propylene (MTP) process produces ethylene and propylene as the main products [2,3]. However, the C₄ fraction, which was produced from naphtha cracking as a co-product of ethylene and propylene, has to be produced from petroleum. Moreover, the booming of the shale gas industry, which produces ethylene and propylene as well, shall further dilute the market share of petroleum-derived light olefins and is expected to reduce the production of C₄. With the abundant coal resources in China, it is necessary and imperative to develop the methanol-to-propylene and -butene (MTPB) technology to counteract the C₄ resource shortfall in the long-term [4].

At present, the fixed-bed reactor MTP process has been developed by employing HZSM-5 zeolite as a catalyst [5,6]. HZSM-5 zeolite has 0.53 × 0.56 nm straight channels and 0.51 × 0.55 nm sinusoidal channels with appropriate acidity, and exhibits high reactivity and good shape-selectivity towards the MTP process [7]. However, due to the diffusion limitation of HZSM-5 zeolite channels to reactants and products, coke deposition on the HZSM-5 surface is very common and eventually lowers the target product selectivity and decreases the catalyst lifetime [8]. HZSM-5 deactivation is mainly attributed to the formation of coke, which is strongly adsorbed by the reactive sites of HZSM-5, i.e., Brønsted and Lewis acid sites, and prevents the access of reactants and hinders the diffusion of the products [9].

The coke location affected the deactivation rate greatly. It is reported that the coke mainly formed inside the micropores of HZSM-5 zeolite and resulted in deactivation [10–12]. Some other researchers found that the coke was more heavily deposited on the external surface of HZSM-5 zeolite and resulted in a fast deactivation due to blocking of the pore mouth [13–15]. It is important to investigate how the coke deposit location affects the catalytic performance of HZSM-5 zeolite.

In comparison with the micro-sized HZSM-5 crystal, the nano-sized HZSM-5 had a shorter diffusion path and exhibited higher catalytic reactivity, propylene selectivity, and longer catalytic lifetime in the MTP reaction [16–19]. Han et al. reported that the nanoparticles were easily aggregated to form intercrystalline mesopores that enhanced molecule diffusivity and accessibility of the active site to decrease the catalyst deactivation rate [20]. In the present research it was found that there were many reasons for the HZSM-5 deactivation, not only due to the size of particles and the presence of mesopores from the diffusion point of view, but also the $\text{SiO}_2/\text{Al}_2\text{O}_3$ molar ratio from the acidity [21], and other factors, should be considered at the same time, such as acid distribution.

In this study, nano-sized HZSM-5 crystal aggregate was synthesized for the MTPB reaction. The coke deposition on nano-HZSM-5 crystal aggregates was characterized by X-ray diffraction (XRD), scanning electron microscopy (SEM), X-ray fluorescence (XRF), NH_3 temperature-programmed desorption (NH_3 -TPD), X-ray photoelectron spectroscopy (XPS), transmission electron microscopy (TEM), energy dispersive spectrometer (EDS), Brunauer-Emmett-Teller (BET), thermogravimetric analysis (TGA), and nuclear magnetic resonance (NMR). The near-graphite coke deposited on the external surface was firstly discovered by TEM. The results revealed the reasons for the deactivation of the nano-sized ZSM-5 aggregate crystals and could be a guideline for improving the catalyst lifetime and target product selectivity.

2. Results and Discussion

2.1. Structure and Acidity

Figure 1 shows the XRD characterization result of the zeolite samples. The five strongest peaks centred at 7.9° , 8.9° , 23.1° , 23.3° , and 23.9° , corresponding to JCPDS card No. 44-0003, were found in all samples, which confirmed the MFI structure of the HZSM-5 zeolite.

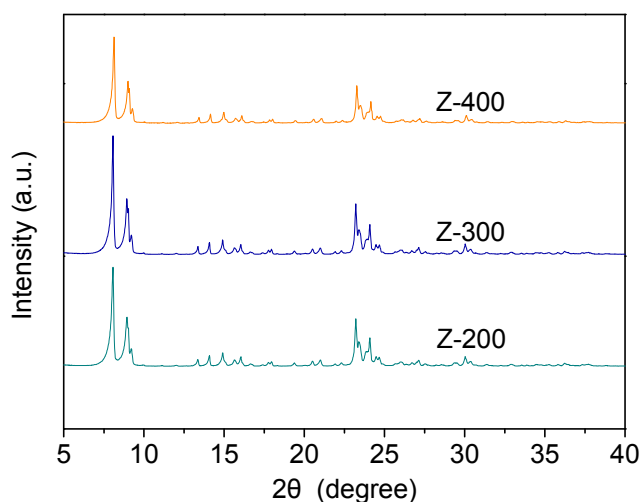


Figure 1. XRD patterns of Z-200, Z-300, and Z-400.

From the SEM images shown in Figure 2, the average particle size of all HZSM-5 zeolites was about $1.3\ \mu\text{m}$ by the agglomeration of smaller primary crystals, the average primary crystal size was about $90\ \text{nm}$, and showed a similar spherical morphology. Further XRF confirmed the as-synthesized zeolites have $\text{SiO}_2/\text{Al}_2\text{O}_3$ molar ratios of 194, 281, and 365, respectively. In addition, the measured

$\text{SiO}_2/\text{Al}_2\text{O}_3$ molar ratios were lower than the corresponding recipe values, and the difference between measured values and recipe values increased with the $\text{SiO}_2/\text{Al}_2\text{O}_3$ molar ratio, which indicated that the utilization of silicon source decreased with the increase of $\text{SiO}_2/\text{Al}_2\text{O}_3$ molar ratio. Two desorption peaks of all samples around 165 °C and 350 °C were observed over the NH_3 -TPD profile in Figure 3, corresponds to NH_3 desorption from weak acid sites and strong acid sites, respectively [22]. As the existence of Al is the origin of HZSM-5 acidity, the total acid sites of the sample generally increase with the decrease of $\text{SiO}_2/\text{Al}_2\text{O}_3$ molar ratio, as shown in Figure 3.

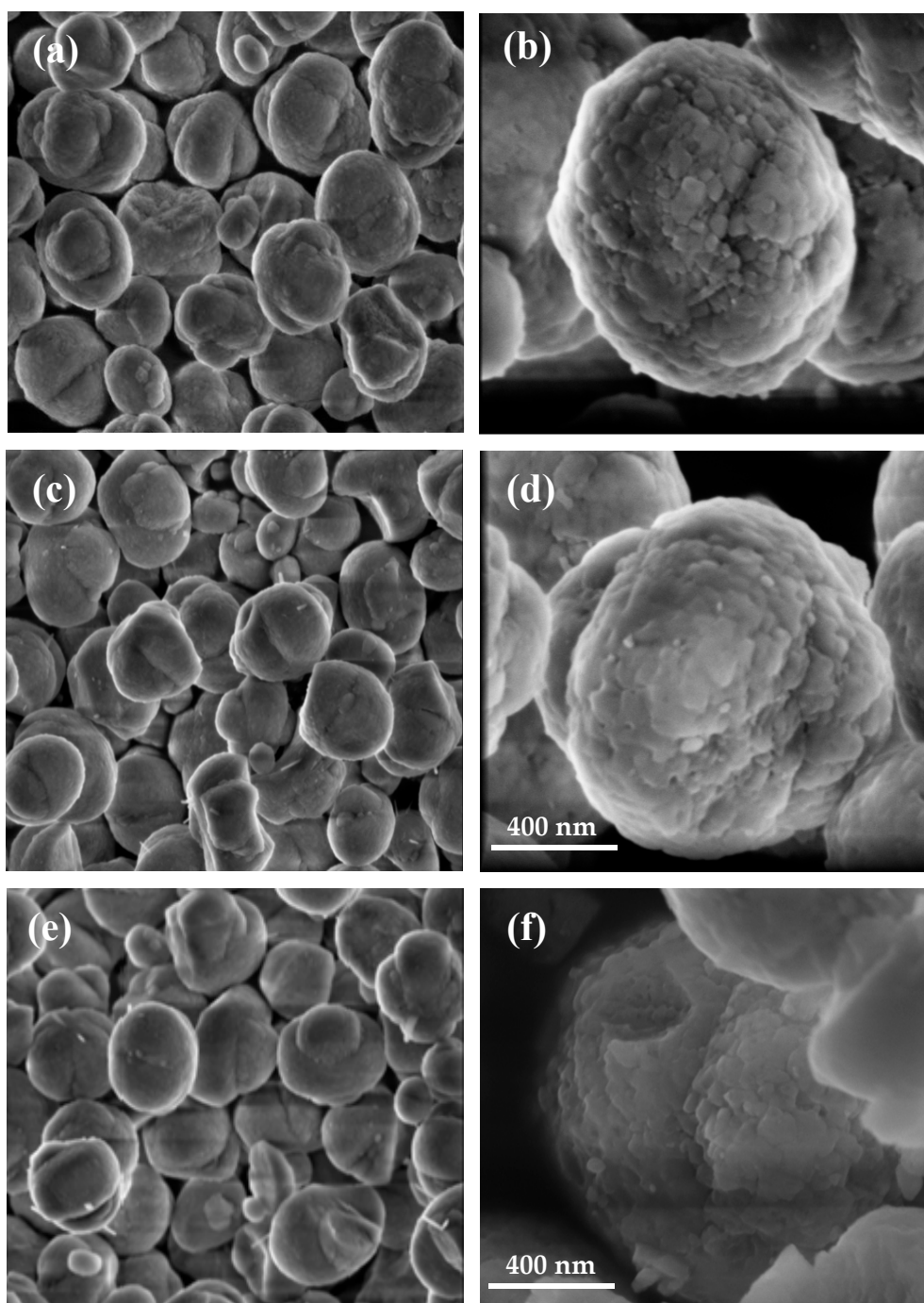


Figure 2. SEM images of Z-200 (a,b), Z-300 (c,d), and Z-400 (e,f) with different magnification.

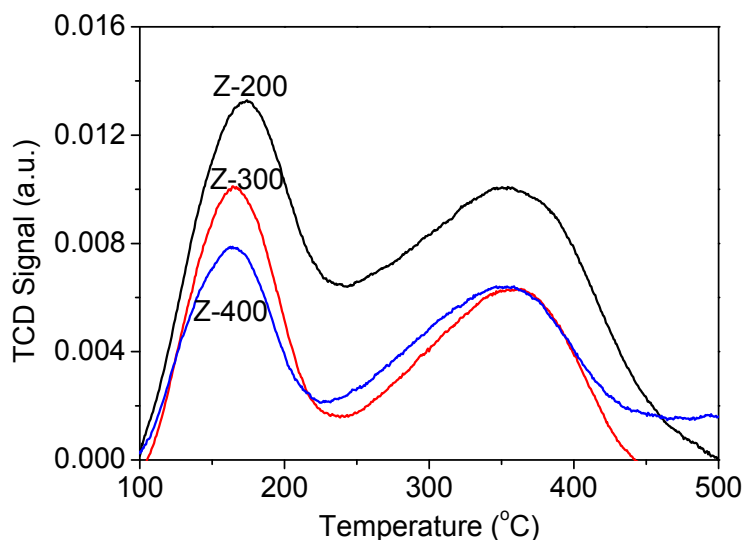


Figure 3. NH_3 -TPD profiles of Z-200, Z-300, and Z-400.

To check the $\text{SiO}_2/\text{Al}_2\text{O}_3$ molar ratio changes of the inner layer and outer shell of the HZSM-5, the crystals were crushed to expose the interior part of zeolites and the as-synthesized zeolites were analyzed by XPS technology, the results of which are shown in Figures 4 and 5. The XPS results only give information about the very outermost surface layer (10 nm) elements of the samples, while the overall element composition of the sample was given by the XRF results. As shown in Figure 4, the $\text{SiO}_2/\text{Al}_2\text{O}_3$ molar ratios of the as-synthesized ZSM-5 determined by XPS were obviously lower than the XRF results with the $\text{SiO}_2/\text{Al}_2\text{O}_3$ molar ratio increasing, disclosing that the exterior shell had more abundant Al with the increase of $\text{SiO}_2/\text{Al}_2\text{O}_3$. Meanwhile, the XPS results of the as-synthesized and crushed ZSM-5 showed that the low $\text{SiO}_2/\text{Al}_2\text{O}_3$ molar ratio (200, 300) slightly increased after crushing, while the high $\text{SiO}_2/\text{Al}_2\text{O}_3$ molar ratio (400) greatly increased after crushing, as shown in Figures 4 and 5. Al distribution in Z-400 was significantly heterogeneous and its surface was distinctly richer in Al than its bulk phase [23,24]. Therefore, more acid sites existed on the exterior shell of Z-400 than the interior.

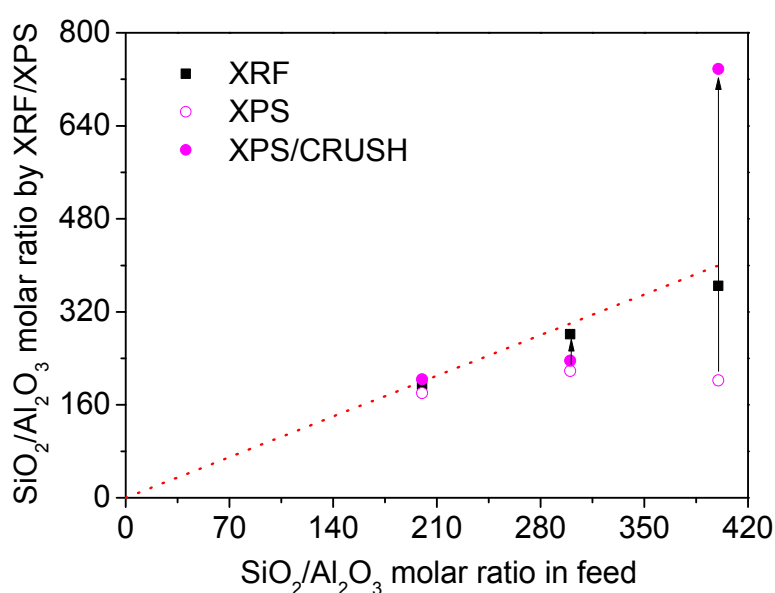


Figure 4. $\text{SiO}_2/\text{Al}_2\text{O}_3$ molar ratio changes of samples by XRF/XPS.

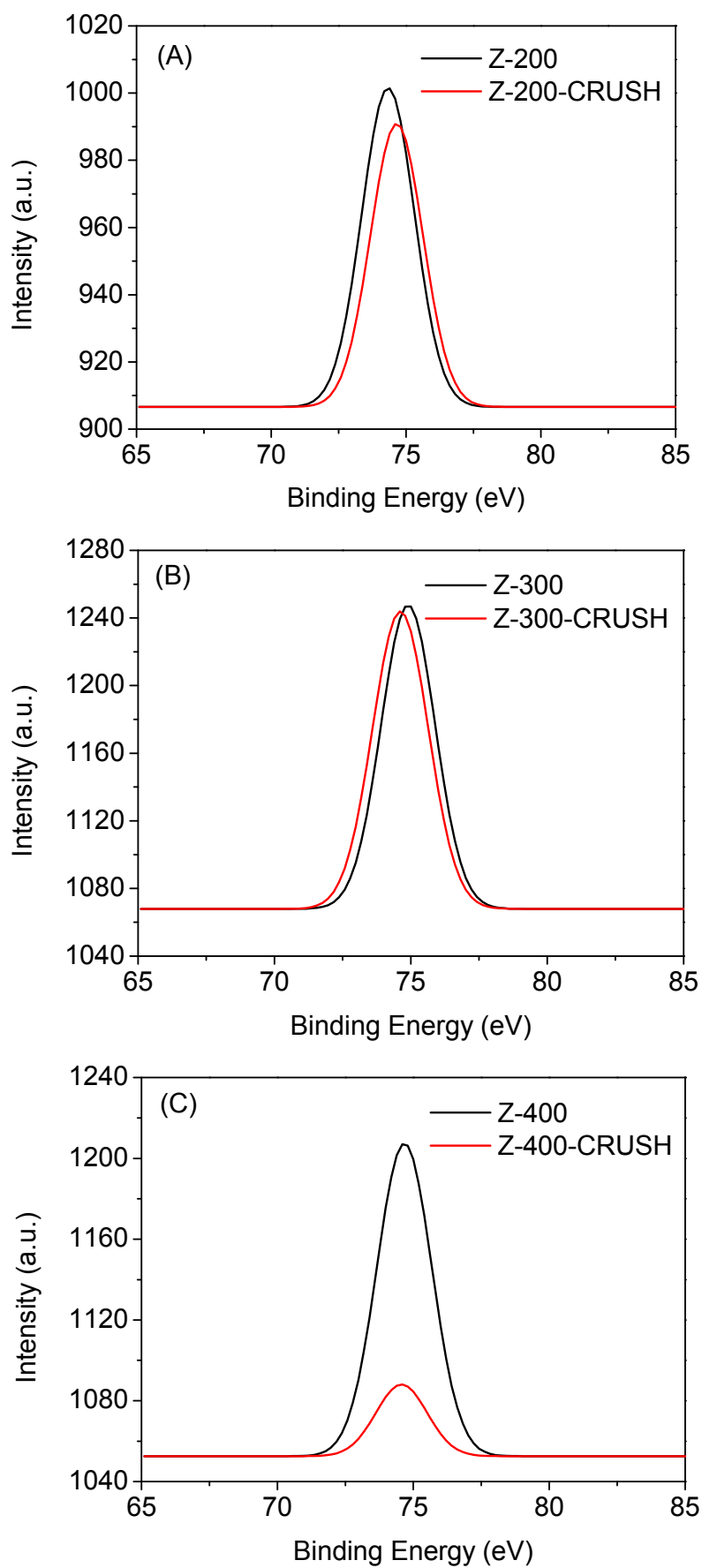


Figure 5. Normalized Al 2p XPS spectra changes of (A) Z-200, (B) Z-300, and (C) Z-400 after crushing.

2.2. Catalytic Performance

Catalyst evaluation results of HZSM-5 zeolites for MTPB reaction were shown in Table 1. In the initial stage, 100% methanol conversion was observed over all samples. As the reaction progressed, methanol conversion decreased gradually, and the lifetime of Z-200, Z-300, and Z-400 was 20 h, 28 h, and 32 h, respectively. In the whole life span of the catalyst, the weight of methanol that each gram of catalyst can process was 60, 84, and 96 g for Z-200, Z-300, and Z-400, respectively. This indicated that the higher SiO₂/Al₂O₃ molar ratio HZSM-5 had the capability of converting methanol to light olefins more efficiently and was more durable than low SiO₂/Al₂O₃ molar ratio samples.

Table 1. Catalytic performance of HZSM-5 zeolites for MTPB reaction (reaction temperature: 480 °C; methanol WHSV: 3 h⁻¹).

Product Selectivity (%) ^a	Z-200	Z-300	Z-400
C ₃ H ₆	29.5	37.6	42.9
C ₄ H ₈	14.5	19.6	21.7
C ₅ H ₁₀	4.6	5.2	6.6
C ₆ ⁺	7.2	7.7	8.4
C ₂ H ₄	10.0	8.6	7.2
C ₂ H ₆	0.11	0.08	0.07
C ₃ H ₈	1.2	1.0	0.77
C ₄ H ₁₀	4.6	4.3	3.3
Lifetime (h) ^b	20	28	32
Methanol/catalyst ratio ^c	60	84	96

Note: ^a The selectivity for propylene and butene were obtained at reaction time of 15 h; ^b The lifetime is defined as the time needed for methanol conversion below 99%; ^c Defined as weight of methanol processed by the catalyst divided by weight of catalyst used for the test.

It was also noticed with the increase of SiO₂/Al₂O₃ molar ratio, which always means fewer acid sites for the reaction (see Figure 3), that the selectivity for propylene increased from 29.5% to 42.9% and the selectivity for butene (including *t*-2-C₄H₈, 1-C₄H₈, *i*-C₄H₈, and *c*-2-C₄H₈) increased from 14.5% to 21.7%. In addition, the pentene selectivity and C₆⁺ hydrocarbon selectivity increased, while the ethylene selectivity, ethane selectivity, propane selectivity, and butane selectivity decreased with the SiO₂/Al₂O₃ molar ratio increase. These results were considered to be a result of the decrease of acid site density in high SiO₂/Al₂O₃ molar ratio samples, which may restrain the hydrogen transfer, oligomerization and aromatization reactions [25]. Therefore, the Z-400 showed the highest selectivity for propylene and butene, the highest methanol/catalyst ratio, and the longest lifetime.

2.3. Coke Formation on HZSM-5

TEM images of fresh and spent Z-400 with different magnifications are shown in Figure 6. By contrast, one can easily find the spent Z-400 (Figure 6b) showing less ordered carbonaceous deposits with a space around 0.33 nm at the edge of the crystal, indicating the formation of near-graphite carbonaceous species. EDS images further confirmed the existence of these graphite species, as shown in Figure 6d. Before the reaction, the external surface of fresh Z-400 was free of coverage. However, after the reaction, it is obvious the external surface of the sample was covered by the graphite carbon, which led to the deactivation of zeolite.

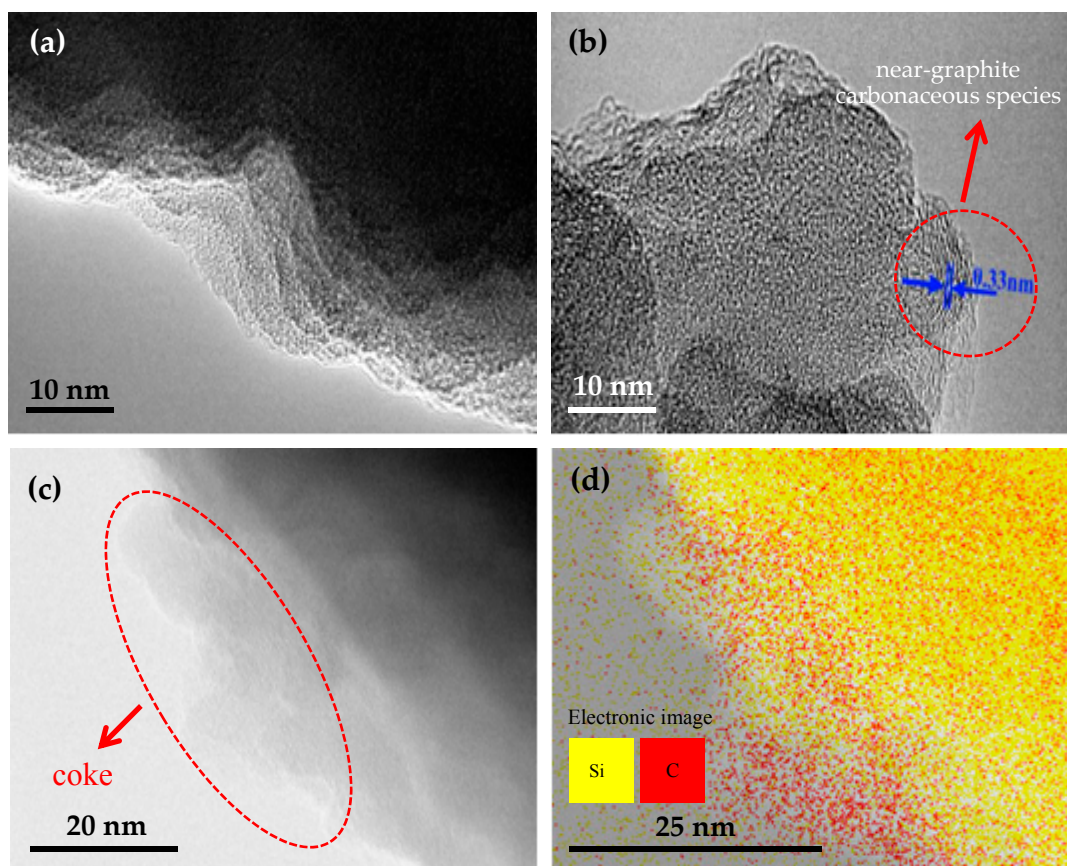


Figure 6. TEM images of (a) fresh Z-400, and (b,c) coke Z-400 for MTPB process at reaction time 46 h (reaction temperature: 480 °C, methanol WHSV: 3 h⁻¹), and (d) EDS image of (c).

Li et al. [26] reported that owing to the passivation of external surface, the modified HZSM-5 zeolite showed higher aliphatic selectivity, but lower aromatic selectivity, than the parent HZSM-5 zeolite in methanol-to-hydrocarbon reactions, suggesting the occurrence of higher olefin aromatization on the external surface of HZSM-5. In addition, it was also discovered that the selectivity to olefins significantly increased over the modified HZSM-5 zeolite, while that of alkanes decreased, which indicated that the external surface was an important place for the formation of alkanes [26]. Regarding the formation of near-graphite carbonaceous deposits on the external surface, we believed it was a result of the coke precursor that was not easy to continuously react due to the poor internal Al distribution. The products diffused from the micropores and re-adsorption occurred on the Z-400 external surface with a large number of acid sites, where continuous oligomerization, cyclization dehydrogenation to aromatics, and condensation reactions occurred to form polycyclic aromatics, and eventually led to the formation near-graphite carbonaceous deposit.

N₂ adsorption-desorption isotherms of fresh and coked Z-400 are shown in Figure 7. The N₂ adsorption-desorption isotherms of fresh Z-400 combined type I and type IV, indicating the formation of intercrystalline mesopores in the sample. Over the spent Z-400 catalyst, the N₂ adsorption-desorption isotherms changed to type I with the absence of hysteresis rings, as well as the decrease of micropore volume, suggesting the deposition of coke in the micropores and intercrystalline mesopores. The specific surface area and pore volume data of fresh and coked Z-400 were listed in Table 2, after the reaction, the obvious decreases of S_{BET} , S_{micro} , S_{exter} , V_{tot} , V_{micro} , and V_{meso} of Z-400 were observed. It is believed that the coke formed in the channels of HZSM-5, which occupied/blocked part of the channel space and, hence, the decrease of the micropore surface and volume, as shown in Table 2. About a 50% and 30% decrease in mesopore volume and micropore volume, respectively, was observed.

As HZSM-5 is a microporous zeolite and its mesopores are created by the aggregate of tiny crystals, this indicated that coke formation on the external surface was more serious than in that in micropores. In addition, Z-200 and Z-300 showed a similar phenomenon. Meanwhile, the decreasing V_{meso} values of Z-200 and Z-300 were lower than Z-400, while the decreasing V_{micro} values of Z-200 and Z-300 were higher than Z-400. These results further suggested greater coke deposition on the external surface of Z-400 than on Z-200 and Z-300. Nevertheless, greater coke deposition in the micropores of Z-200 and Z-300 than Z-400. These results could be attributed to the coke precursor being easy to continuously react to form coke in the micropores of Z-200 and Z-300 due to a large amount of internal Al, while the coke precursor was easy to continuously react to form coke on the external surface of Z-400 due to a large amount of external Al with little internal Al.

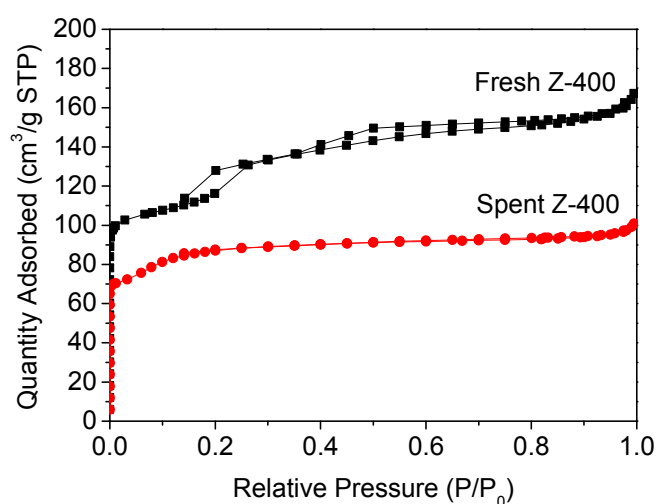


Figure 7. N_2 adsorption-desorption isotherms of fresh Z-400 and spent Z-400 for MTPB process at reaction time 46 h (reaction temperature: 480 °C, methanol WHSV: 3 h⁻¹).

Table 2. Textural parameters of fresh and coke deposited HZSM-5 zeolites for MTPB process at reaction time of 46 h (reaction temperature: 480 °C; methanol WHSV: 3 h⁻¹).

Samples	S_{BET} (m ² /g)	S_{micro} (m ² /g)	S_{exter} (m ² /g)	V_{tot} (cm ³ /g)	V_{micro} (cm ³ /g)	V_{meso} (cm ³ /g)
Fresh Z-200	451.7	300.8	150.9	0.275	0.119	0.156
Coke deposited Z-200	299.2	68.0	231.2	0.173	0.030	0.143
Fresh Z-300	431.2	268.7	162.5	0.305	0.109	0.196
Coke deposited Z-300	311.8	26.6	285.2	0.171	0.027	0.144
Fresh Z-400	435.9	262.6	173.3	0.259	0.103	0.156
Coke deposited Z-400	303.4	177.7	125.7	0.156	0.080	0.076

The pore size distribution of fresh and spent Z-400 is shown in Figure 8. After the reaction, it was clearly seen the narrowing of mesopore from 3.25 to 4 nm to 2.5 to 3.25 nm, and a significant mesopore volume decrease. These results further indicated that a certain amount of coke deposited in the intercrystalline mesopores, where the mesopores' surface is the external surface of very small primary crystals.

The thermogravimetric analysis-derivative thermogravimetric analysis (TGA-DTG) profiles of deactivated Z-200, Z-300, and Z-400 are shown in Figure 9. Approximately 10%, 10%, and 8% weight loss of Z-200, Z-300 and Z-400, respectively, between 420 °C and 680 °C was observed, which was ascribed to the coke combustion of the deactivated HZSM-5. The higher DTG peak temperature of Z-400 than Z-200 and Z-300 showed the coke species were difficult to combust, which was consistent with the near-graphite carbonaceous species on the external surface of Z-400 as discerned by TEM. The amounts of coke on the external surface and in the micropores were calculated by the method in [27]. The coke formation inside the micropores was calculated from a decrease in micropore volume,

assuming coke has a density of 1.22 g/cm^3 . The coke content deposited on the external surface was calculated by subtracting the internal coke content from the total coke content. As shown in Table 3, coke deposited on the external surface accounted for 1.8%, 9.8%, and 67.8% of the total coke of Z-200, Z-300, and Z-400, respectively, while coke deposited in the micropores accounted for 98.2%, 90.1%, and 32.2% of the total coke of Z-200, Z-300, and Z-400, respectively. These results further indicated that coke preferred to form in the micropores of Z-200 and Z-300, while coke preferred to form on the external surface and intercrystalline mesopores of Z-400. The higher coke content in the micropore of Z-200 and Z-300 than Z-400 might be due to the coke precursor continuously reacting on these acid sites to form coke in the micropores. While coke preferred to form on the external surface of Z-400, this was attributed to the distinctly rich Al shell with a poor Al core, resulting in the non-shape-selective side reactions of product diffusion from the micropores on the large number of acid sites on the external surface.

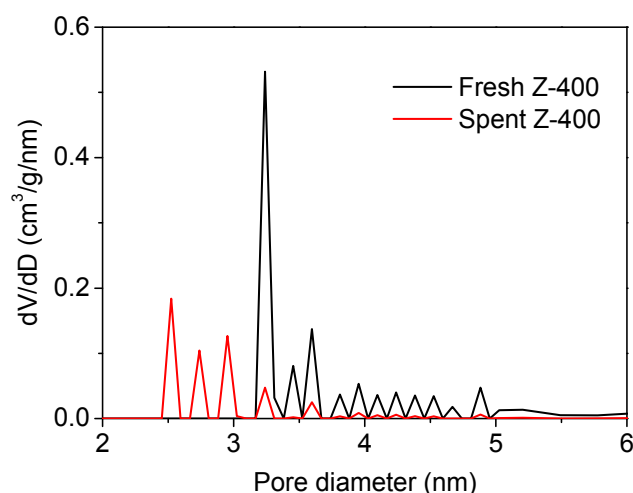


Figure 8. Pore size distributions of fresh Z-400 and spent Z-400 for MTPB process at reaction time 46 h (reaction temperature: $480 \text{ }^\circ\text{C}$, methanol WHSV: 3 h^{-1}).

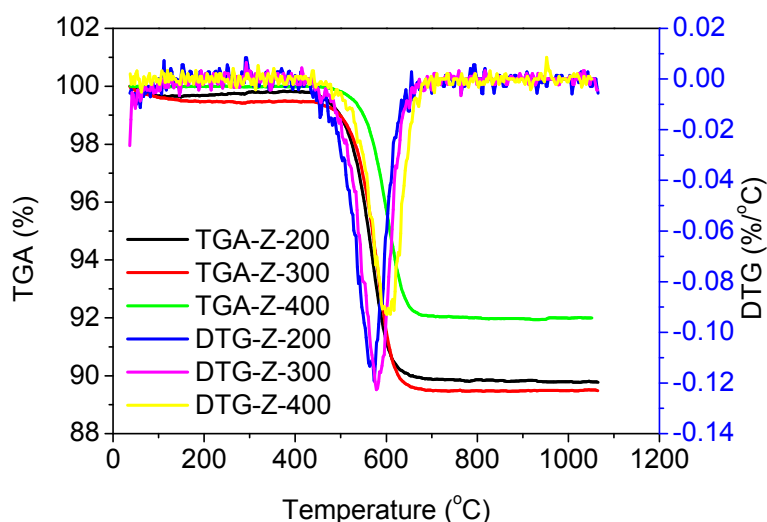


Figure 9. TGA-DTG patterns of coke HZSM-5 zeolites for MTPB process at reaction time 46 h (reaction temperature: $480 \text{ }^\circ\text{C}$; methanol WHSV: 3 h^{-1}).

Table 3. Coke content of HZSM-5 zeolites for MTPB process at reaction time of 46 h (reaction temperature: 480 °C; methanol WHSV: 3 h⁻¹).

Sample	Total Coke (%)	Coke Inside Micropore (g _{coke} /g _{cat})	Coke on External Surface (g _{coke} /g _{cat})
Z-200	11.1	0.109	0.002
Z-300	11.1	0.100	0.011
Z-400	8.7	0.028	0.059

Figure 10 showed the ¹³C MAS NMR spectrum of spent Z-400. There were a major signal around 128 ppm and minor signals around 32 ppm and 20 ppm, which were attributed to a mixture of C₆–C₁₂ aromatics and paraffins, such as polymethylbenzenes (134 ppm, 129 ppm, and 21 ppm), and 2,3-hexadiene (132–134 ppm, 126–128 ppm, and ca. 18 ppm) [28]. These molecules were proposed to be the main components of carbonaceous deposits over HZSM-5.

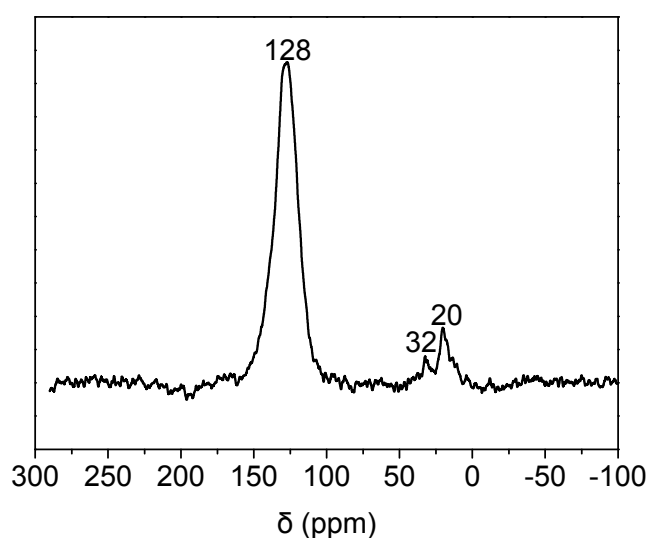


Figure 10. ¹³C MAS NMR spectrum of coke Z-400 for MTPB process at reaction time of 46 h (reaction temperature: 480 °C; methanol WHSV: 3 h⁻¹).

3. Experimental

3.1. Catalyst Preparation

The aggregates of nano-sized HZSM-5 zeolite crystals were prepared as follows: TPAOH aqueous solution, H₂O, NaOH, and NaAlO₂ were mixed under agitation for 1 h before adding 30% silica sol. This obtained mixture was stirred at room temperature for 24 h. The sol was charged into Teflon-lined stainless-steel autoclaves and crystallized under autogenous pressure at 125 °C for 72 h. After that, the solid product was separated by centrifugation, and washed thoroughly with DI water. Then the obtained paste was dried overnight at 120 °C and calcined in air at 550 °C for 12 h. Finally, the samples were triple ion-exchanged with a 1.0 mol/L ammonium nitrate (NH₄NO₃) solution at 80 °C for 2 h and separated by centrifugation and followed by drying and calcination at 550 °C in air for 10 h. For the starting sol of nano-sized HZSM-5 crystals aggregate preparation, the molar ratio of x SiO₂:Al₂O₃:0.1 x TPAOH:0.038 x Na₂O:13.5 x H₂O was set by changing the SiO₂/Al₂O₃ molar ratio of 200, 300, and 400, respectively, and the synthesized samples were named as Z-200, Z-300, and Z-400, accordingly.

3.2. Catalyst Characterization

X-ray diffraction (XRD) analysis was tested on a D8 ADVANCE (Bruker AXS, Karlsruhe, Germany) X-ray diffractometer system (40 kV, 40 mA) in the 2θ range of 5–90°. X-ray fluorescence (XRF) analysis

was tested on a ZSX Primus II (Rigaku, Tokyo, Japan) X-ray fluorescence spectrometer (4 kW) using an Rh target to obtain the SiO₂/Al₂O₃ molar ratio of the sample. X-ray photoelectron spectroscopy (XPS) analysis was performed on a Thermo Scientific ESCALAB 250Xi (Thermo Fisher Scientific, Waltham, MA, USA) X-ray photoelectron spectrograph to obtain the content of Al on the surface of the sample. Scanning electron microscopy (SEM) was performed with a Nova NanoSEM 450 (FEI, Brno, Czech Republic) scanning electron microscope (acceleration voltage: 30 V–30 kV) to examine the surface topography and size of the sample. Transmission electron microscopy (TEM) and energy dispersive spectrometer (EDS) were operated at 120 kV on a JEM ARM200F (JEOL, Tokyo, Japan) transmission electron microscope. Prior to the test, the sample was uniformly dispersed in ethanol with ultrasonication to obtain a well-dispersed suspension. The suspension was subsequently added dropwise onto a copper grid.

NH₃ temperature-programmed desorption (NH₃-TPD) was carried out using an AutoChem II 2920 (Micromeritics, Atlanta, GA, USA) chemical adsorption instrument. A 100 mg sample was placed in a quartz tubular reactor and pre-treated at 550 °C with He flow for 30 min and then cooled to 100 °C. Then, diluted NH₃ (10 v/v% NH₃ in helium) was introduced into the reactor for 80 min at 100 °C, followed by purging with He flow for 20 min to remove the physically adsorbed NH₃ and to obtain a smooth and steady baseline. Finally, the sample was heated at a ramp rate of 10 °C/min from 100 °C to 600 °C and the desorbed ammonia signal was detected by a thermal conductivity detector (TCD). N₂ adsorption-desorption measurement was performed on an ASAP2460 (Micromeritics, Atlanta, GA, USA) instrument at 77 K. Before the test, the samples were degassed in vacuum for 3 h at 573 K. The total specific surface area (S_{BET}) was determined by the Brunauer-Emmett-Teller (BET) method based on the P/P₀ data in the range of 0.007 to 0.02. The micropore volume (V_{micro}) and external specific surface area (S_{exter}) were obtained from the t-plot method. A single point desorption pore volume at P/P₀ = 0.99 was used to obtain the total pore volume (V_{tot}). The micropore specific surface area (S_{micro}) was obtained by subtracting the external specific surface area from the total specific surface area, and the mesopore volume (V_{meso}) was obtained by subtracting the micropore volume from the total pore volume. A non-local-density-functional-theory (NLDFT) model was used to obtain the pore size distribution. Thermogravimetric analysis (TGA) was carried out using a STA 449F3 (NETZSCH, Selb, Germany) simultaneous thermal analyser with an air flow of 20 mL/min and a temperature ramp rate of 10 °C/min from room temperature to 1000 °C. ¹³C magic angle spinning nuclear magnetic resonance (¹³C MAS NMR) was performed on a NMR 400 M (WB) system (Bruker, Karlsruhe, Germany) (Avance III HD/89 mm). The cross-polarization (CP) technique was applied to the ¹³C MAS NMR experiment.

3.3. Catalyst Evaluation

The MTPB reaction was carried out in a fixed-bed micro-reactor (Beijing Mingrui Boyuan Technology Development Co. Ltd., Beijing, China). In each run, 1.0 g of catalyst (pelletized and cracked to 20–40 meshes) and 4 g of quartz sand were loaded in the center of a 10 mm i.d. stainless steel tube reactor and activated in a 150 mL/min nitrogen flow at 500 °C for 30 min. Then, the diluted methanol (80 wt % in water) solution, which was diluted with a nitrogen flow of 150 mL/min, was fed into a 480 °C reactor at atmospheric pressure. Weight hourly space velocity (WHSV) was kept at 3 h⁻¹. (Agilent 7890A) (Agilent Technologies, Palo Alto, CA, USA) gas chromatograph equipped with a HP-PLOT Al₂O₃/KCl column (50 m × 0.53 mm × 15 μm) to separate C₁–C₆ hydrocarbons, and a HP-PLOT Q column (30 m × 320 μm × 20 μm) to separate alcohols and ethers, as well as a 6' × 1/8'' Hayesep Q column and a 10' × 1/8'' 13X zeolite column to separate the permanent gases, such as CO, CO₂, and H₂, etc. Two flame ionization detectors (FID) and a thermal conductivity detector (TCD) were used to detect products. Methanol conversion (X) and selectivity of the products (S) were defined as follows:

$$X = \frac{n_{MeOH}^i - n_{MeOH}^o - 2n_{DME}^o}{n_{MeOH}^o} \times 100\% \quad (1)$$

$$S = \frac{m \times n_{C_m H_n}^o}{n_{MeOH}^i - n_{MeOH}^o - 2n_{DME}^o} \times 100\% \quad (2)$$

the n is the number of moles, the superscripts i and o denote the components at the inlet and outlet of reactor, respectively, and the m is the number of carbon atoms corresponding to $C_m H_n$.

4. Conclusions

Nanocrystal HZSM-5 zeolite aggregates with different $\text{SiO}_2/\text{Al}_2\text{O}_3$ molar ratios were prepared for MTPB reactions. Near-graphite carbonaceous deposition on the external surface of nanocrystal HZSM-5 zeolite aggregates ($\text{SiO}_2/\text{Al}_2\text{O}_3$ molar ratio = 400) was observed by TEM and EDS. The acid site distribution could significantly affect the catalytic performance and coke formation. Coke preferred to deposit in the micropores of the low $\text{SiO}_2/\text{Al}_2\text{O}_3$ molar ratio samples (200, 300) with relatively uniform Al distribution, while coke preferred to deposit on the external surface and in the intergranular spaces of the high $\text{SiO}_2/\text{Al}_2\text{O}_3$ molar ratio sample (400) with an obviously poor Al core and a rich Al shell.

Acknowledgments: This work is supported by the Science and Technology Innovation Project of Shenhua Group (No.: ST930014SH03).

Author Contributions: Yu Sang has made substantial contributions to the conception or design of the work, and the acquisition, analysis, and interpretation of data for the work. She has drafted the work. She has made the final approval of the version to be published. She has agreed to be accountable for all aspects of the work in ensuring that questions related to the accuracy or integrity of any part of the work are appropriately investigated and resolved. Aihua Xing, Chuanfu Wang, Zhihua Han and Yulong Wu have made substantial contributions to the interpretation of data for the work. They have revised the work critically for important intellectual content. They have made the final approval of the version to be published. They have agreed to be accountable for all aspects of the work in ensuring that questions related to the accuracy or integrity of any part of the work are appropriately investigated and resolved.

Conflicts of Interest: The authors declare no conflict of interest.

References

1. Firoozi, M.; Baghalha, M.; Asadi, M. The effect of micro and nano particle sizes of H-ZSM-5 on the selectivity of MTP reaction. *Catal. Commun.* **2009**, *10*, 1582–1585. [[CrossRef](#)]
2. Yaripour, F.; Shariatnia, Z.; Sahebdelfar, S.; Irandoukht, A. Conventional hydrothermal synthesis of nanostructured H-ZSM-5 catalysts using various templates for light olefins production from methanol. *J. Nat. Gas Sci. Eng.* **2015**, *22*, 260–269. [[CrossRef](#)]
3. Losch, P.; Boltz, M.; Louis, B.; Chavan, S.; Olsbye, U. Catalyst optimization for enhanced propylene formation in the methanol-to-olefins reaction. *Comptes Rendus Chim.* **2015**, *18*, 330–335. [[CrossRef](#)]
4. Xing, A.H.; Zhang, X.F.; Suo, Y.; Feng, Q.Y.; Shi, Y.L. Comprehensive utilization and prospect of C4 hydrocarbon. *Clean Coal Technol.* **2015**, *21*, 66–71.
5. Hadi, N.; Niaei, A.; Nabavi, S.R.; Farzi, A.; Shirazia, M.N. Development of a New Kinetic Model for Methanol to Propylene Process on Mn/H-ZSM-5 Catalyst. *Chem. Biochem. Eng. Q.* **2014**, *28*, 53–63.
6. Mokrani, T.; Scurrrell, M. Gas conversion to liquid fuels and chemicals: The methanol route-catalysis and processes development. *Catal. Rev.* **2009**, *51*, 1–145. [[CrossRef](#)]
7. Yong, X.J.; Du, Z.P.; Li, Y.; Luo, C.T. Application status of Lurgi methanol to propylene technology and development of key catalyst. *Technol. Dev. Chem. Ind.* **2013**, *42*, 18–21.
8. Li, H.S.; He, S.C.; Ma, K.; Wu, Q.; Jiao, Q.Z.; Sun, K.N. Micro-mesoporous composite molecular sieves H-ZSM-5/MCM-41 for methanol dehydration to dimethyl ether: Effect of $\text{SiO}_2/\text{Al}_2\text{O}_3$ ratio in H-ZSM-5. *Appl. Catal. A* **2013**, *450*, 152–159. [[CrossRef](#)]
9. Mores, D.; Stavitski, E.; Kox, M.H.F.; Kornatowski, J.; Olsbye, U.; Weckhuysen, B.M. Space- and Time-Resolved In-situ Spectroscopy on the Coke Formation in Molecular Sieves: Methanol-to-Olefin Conversion over H-ZSM-5 and H-SAPO-34. *Chem. Eur. J.* **2008**, *14*, 11320–11327. [[CrossRef](#)] [[PubMed](#)]
10. Bibby, D.M.; Howe, R.F.; McLellan, G.D. Coke formation in high-silica zeolites. *Appl. Catal. A* **1992**, *93*, 1–34. [[CrossRef](#)]

11. Rownaghi, A.A.; Rezaei, F.; Hedlund, J. Uniform mesoporous ZSM-5 single crystals catalyst with high resistance to coke formation for methanol deoxygenation. *Microporous Mesoporous Mater.* **2012**, *151*, 26–33. [[CrossRef](#)]
12. Bibby, D.M.; Milestone, N.B.; Patterson, J.E.; Aldridge, L.P. Coke formation in zeolite ZSM-5. *J. Catal.* **1986**, *97*, 493–502. [[CrossRef](#)]
13. Sexton, B.A.; Hughes, A.E.; Bibby, D.M. An XPS study of coke distribution on ZSM-5. *J. Catal.* **1988**, *109*, 126–131. [[CrossRef](#)]
14. Guisnet, M.; Magnoux, P. Organic chemistry of coke formation. *Appl. Catal. A* **2001**, *212*, 83–96. [[CrossRef](#)]
15. Kim, J.; Choi, M.; Ryoo, R. Effect of mesoporosity against the deactivation of MFI zeolite catalyst during the methanol-to-hydrocarbon conversion process. *J. Catal.* **2010**, *269*, 219–228. [[CrossRef](#)]
16. Hu, Z.; Zhang, H.; Wang, L.; Zhang, H.; Zhang, Y.; Xu, H.; Shen, W.; Tang, Y. Highly stable boron-modified hierarchical nanocrystalline ZSM-5 zeolite for the methanol to propylene reaction. *Catal. Sci. Technol.* **2014**, *4*, 2891–2895. [[CrossRef](#)]
17. Ahmadpour, J.; Taghizadeh, M. Catalytic conversion of methanol to propylene over high-silica mesoporous ZSM-5 zeolites prepared by different combinations of mesogenous templates. *J. Nat. Gas Sci. Eng.* **2015**, *23*, 184–194. [[CrossRef](#)]
18. Kim, Y.; Kim, J.C.; Jo, C.; Kim, T.W.; Kim, C.U.; Jeong, S.Y.; Chae, H.J. Structural and physicochemical effects of MFI zeolite nanosheets for the selective synthesis of propylene from methanol. *Microporous Mesoporous Mater.* **2016**, *222*, 1–8. [[CrossRef](#)]
19. Hu, S.; Shan, J.; Zhang, Q.; Wang, Y.; Liu, Y.S.; Gong, Y.J.; Wu, Z.J.; Dou, T. Selective formation of propylene from methanol over high-silica nanosheets of MFI zeolite. *Appl. Catal. A* **2012**, *445*, 215–220. [[CrossRef](#)]
20. Han, W.; Jia, Y.X.; Xiong, G.X.; Yang, W.S. Hydrothermal Stability of Meso-microporous Composites and Their Catalytic Cracking Performance. *Chin. J. Catal.* **2011**, *32*, 418–427. [[CrossRef](#)]
21. Sang, Y.; Jiao, Q.; Li, H.; Wu, Q.; Zhao, Y.; Sun, K. HZSM-5/MCM-41 composite molecular sieves for the catalytic cracking of endothermic hydrocarbon fuels: Nano-ZSM-5 zeolites as the source. *J. Nanopart. Res.* **2014**, *16*, 1–11. [[CrossRef](#)]
22. Rownaghi, A.A.; Hedlund, J. Methanol to gasoline-range hydrocarbons: Influence of nanocrystal size and mesoporosity on catalytic performance and product distribution of ZSM-5. *Ind. Eng. Chem. Res.* **2011**, *50*, 11872–11878. [[CrossRef](#)]
23. Hughes, A.E.; Wilshier, K.G.; Sexton, B.A.; Smart, P. Aluminum distribution in ZSM-5 as determined by X-ray photoelectron spectroscopy. *J. Catal.* **1983**, *80*, 221–227. [[CrossRef](#)]
24. Wang, C.F.; Zhang, Q.; Zhu, Y.F.; Zhang, D.K.; Chen, J.Y.; Chiang, F.K. p-Xylene selectivity enhancement in methanol toluene alkylation by separation of catalysis function and shape-selective function. *Mol. Catal.* **2017**, *433*, 242–249. [[CrossRef](#)]
25. Wang, Q.Y.; Xu, S.T.; Chen, J.R.; Wei, Y.X.; Li, J.Z.; Fan, D.; Yu, Z.X.; Qi, Y.; He, Y.L.; Xu, S.L.; et al. Synthesis of mesoporous ZSM-5 catalysts using different mesogenous templates and their application in methanol conversion for enhanced catalyst lifespan. *RSC Adv.* **2014**, *4*, 21479–21491. [[CrossRef](#)]
26. Li, J.H.; Wang, Y.N.; Jia, W.Z.; Xi, Z.W.; Chen, H.H.; Zhu, Z.R.; Hu, Z.H. Effect of external surface of HZSM-5 zeolite on product distribution in the conversion of methanol to hydrocarbons. *J. Energy Chem.* **2014**, *23*, 771–780. [[CrossRef](#)]
27. Choi, M.; Na, K.; Kim, J.; Sakamoto, Y.; Terasaki, O.; Ryoo, R. Stable single-unit-cell nanosheets of zeolite MFI as active and long-lived catalysts. *Nature* **2009**, *461*, 246–249. [[CrossRef](#)] [[PubMed](#)]
28. Wang, W.; Jiang, Y.J.; Hunger, M. Mechanistic investigations of the methanol-to-olefin (MTO) process on acidic zeolite catalysts by in situ solid-state NMR spectroscopy. *Catal. Today* **2006**, *113*, 102–114. [[CrossRef](#)]

